The Role of Phase Transformation in Electron-Beam Welding of TiAl-Based Alloys

Q. XU, M.C. CHATURVEDI, and N.L. RICHARDS

The weldability of two TiAl-based alloys, Ti-45Al-2Nb-2Mn and Ti-48Al-2Nb-2Mn, was investigated with the electron-beam welding process. It was found that the alloys were susceptible to solid-state cracking due to high thermally induced stresses and, more significantly, to the intrinsic brittleness of the microstructures. This work correlated the quality of the TiAl welds, made using different sets of welding parameters which gave rise to different cooling rates, to the microstructures that developed during welding. It was found that the welds were crack-free if the weld cooling rates were such that decomposition of the high-temperature α phase in the weld was not suppressed. It was shown that the Ti-48Al–based alloy was less susceptible to the solid-state cracking and, thus, was more weldable than the Ti-45Al–based alloy because the α phase in the alloy with a higher aluminum content could decompose more readily. A continuous cooling transformation (CCT) diagram is suggested to be used as an appropriate reference for the selection of welding parameters which induce suitable microstructures in the welds and result in crack-free welds.

I. INTRODUCTION

TiAl-BASED alloys are rapidly emerging as the most attractive alternate structural materials for high-temperature applications in gas turbine engines, owing to their high specific strength and modulus, good creep, and oxidation resistance. The effective utilization of the alloys will, in many cases, have to require joining. Recent research[1–11] has demonstrated that a sound joint can be produced either by fusion-welding processes, including electron-beam welding, gas-tungsten arc welding, laser welding, and linear friction welding, by diffusion bonding, or by brazing, although every process has certain limitations. Patterson *et al.*[1] investigated the electron-beam weldability of a Ti-48 at. pct-6.5 vol pct TiB_2 alloy and observed a susceptibility to solid-state cracking. They suggested that weld cracking could be avoided by selection of welding parameters that would result in the calculated values of average heat-affected zone cooling rates below, approximately, 300 °C/s for their alloy. It was also reported[6] that a crack-free weld could be obtained on a different joining geometry by preheating the workpiece above the brittle-to-ductile transition temperature. Austin *et al.*[4] observed that welds made at elevated temperatures did not crack in the glovebox upon cooling, but would later crack when removed to normal atmospheric conditions. It was believed that the combination of residual stresses and hydrogen in the moist air could be responsible for the cracking of welds. They suggested a stress-relief treatment prior to exposure to the ambient atmosphere.

The present study was a systematic investigation of the microstructures developed in the electron-beam welds of a Ti-45Al-2Nb-2Mn and a Ti-48Al-2Nb-2Mn alloy, with different welding parameters leading to a wide range of cooling rates. Attempt was made to determine the dependence of the solid-state weld cracking susceptibility of TiAl-based alloys on the microstructures of the welds. It was observed that phase transformations that occurred after the welding process played a significant role in controlling the quality of the electron-beam welds. It is, therefore, suggested that the continuous cooling transformation (CCT) diagram could be used as a reference for the selection of welding parameters to control the microstructures and, hence, the cracking susceptibility of welds.

II. EXPERIMENTAL

The chemical analysis of the two TiAl-based alloys used in this research is given in Table I. The Ti-45Al-2Nb-2Mn alloy was cast and heat treated at 1320 °C followed by air cooling. The Ti-48Al-2Nb-2Mn alloy was taken from a 50 kg ingot prepared by plasma arc melting and was heat treated at 1410 °C followed by air cooling. Bead-on-plate weld coupons were approximately 50-mm long, 15-mm wide, and 10-mm thick, and the workpieces for butt welding were approximately 115-mm long, 10-mm wide, and 6-mm thick. They were cut by a slow-speed diamond wheel and were mechanically ground with 180-grit paper, followed by cleaning in ethanol in an ultrasonic bath prior to welding.

Welding trials were conducted using a bead-on-plate technique to derive welding parameters, followed by butt welding using a Sciaky Mark VII electron-beam welding machine, with a beam voltage of 44 kV, at Bristol Aerospace Limited. The beam current varied from 22 to 60 mA, and the welding travel speed varied from 2.1 to 25.4 mm/s. Some of the welding trials were carried out by preheating the weld coupons at temperatures ranging from 230 °C to 600 °C. The preheating was conducted by the use of *in situ* beam rastering. A defocused beam at relatively low power was rastered over the workpieces, and the power and focus condition of the beam were adjusted to reach the desired preheating temperature. Two thermocouples were attached at sides of the weld coupons to monitor the preheating temperature. The welding parameters were adjusted to achieve a

Q. XU, Research Associate, and M.C. CHATURVEDI, Professor, are with the Department of Mechanical and Industrial Engineering, University of Manitoba, Winnipeg, MB, Canada R3T 5V6. N.L. RICHARDS, formerly Manager of Materials and Processes Engineering with Bristol Aerospace Ltd., Winnipeg, Canada, is Adjunct Professor, Department of Mechanical and Industrial Engineering, University of Manitoba, and a Consultant.

Manuscript submitted March 2, 1998.

Table I. Compositions of Parent Materials

Material	Al	Nb	Mn	O	Ti
Ti-45Al-2Nb-2Mn	45.2	2.78	1.89	870 ppm	balance
Ti-48Al-2Nb-2Mn	48.4	2.64	1.91	640 ppm	balance

Table II. Welding Parameters

Beam Voltage (kV)	Beam Current (mA)	Weld Speed (mm/s)	Preheat (°C)	Calculated Cooling Rate (°C/s)
44	60	25.4	25	1670
44	58	25.4	250	1150
44	46	12.7	25	1100
44	45	12.7	250	730
44	28	4.2	25	590
44	25	4.2	600	170
44	26	4.2	500	220
44	26	4.2	480	240
44	22	2.1	25	380
44	27	4.2	320	340
44	27	4.2	270	380
44	27	4.2	230	420
44	26	4.2	430	270
44	26	4.2	500	200

penetration of approximate 5.5 mm in depth for the bead-on-plate weld. Full penetration was attained for all butt welds. That is, the depth of penetration for the bead-on-plate and butt welding was almost the same.

The welds were sliced every 5 mm in length by electro-discharge machining (EDM), and these cross-sectional samples were subsequently mechanically ground and polished. A JEOL* 840 scanning electron microscope was utilized to examine the cross-sectional samples, and the number of cracks that were observed was counted for each weld. The variation in composition within weld fusion zones was characterized on polished cross-sectional samples by an energy-dispersive X-ray spectroscopy (EDS) instrument attached to the JEOL 840 scanning electron microscope.

*JEOL is a trademark of Japan Optics Ltd., Tokyo.

The welding parameters were normalized by the calculated values of the fusion-zone boundary cooling rates, listed in Table II. The cooling rates at fusion-zone boundaries were estimated using a Rosenthal heat-flow analysis[12] and average thermophysical properties for a Ti-50Al alloy[13] and were reported as an average cooling rate over a temperature range from 1350 °C to 1000 °C. Following the analysis, the welding parameters that were selected in this research resulted in a wide range of fusion-zone boundary cooling rates, from 170 °C/s to 1670 °C/s (Table II). Due to the brittleness of the materials, it was not possible to drill holes precisely at the fusion-zone boundaries in order to insert thermal couples to measure the cooling rates. Therefore, cooling rates at the fusion-zone boundaries could not be measured. However, in a previous study, we measured the cooling rates at the fusion-zone boundaries in INCONEL* 718 alloy welds made on similar-size specimens and by similar welding techniques as used in this study. It was found that the observed cooling rates were similar to the calculated values. Therefore, it is assumed that the calculated cooling rates at the fusion-zone boundaries in the present study are also similar to the actual cooling rates. Moreover, the fact that the microstructures that developed in GLEEBLE-simulated specimens at certain measured cooling rates were found to be consistent with those in the welds made at the same calculated values of cooling rates indicates that the calculated values of cooling rates were in reasonable agreement with the actual cooling rates.

*INCONEL is a trademark of INCO Alloys International, Huntington, WV.

A systematic investigation was conducted with a GLEEBLE 1500 thermomechanical simulator to establish critical cooling rates at which different types of microstructures formed when the alloys cooled from the high-temperature α-phase field. The GLEEBLE test pieces were 120-mm long, 10-mm wide, and 3-mm thick. They were cut by EDM and ground with 120-grit paper to eliminate the EDM recast layers. A wide range of cooling rates was attained by regulating the flow of compressed argon, compressed helium, water, and their combinations, which were used as the coolants. Metallographic samples of GLEEBLE test pieces were cut by a spark machine, mechanically ground, and polished. The samples were etched with Kroll's reagent of 7 vol pct HF, 21 vol pct HNO_3, and 72 vol pct H_2O for optical microscopic examination.

Discs of 3 mm in diameter were spark-cut for the transmission electron microscope (TEM) characterization of microstructures that developed in welds and in GLEEBLE-simulated samples. They were ground to ~120 μm in thickness, and the weld samples were further dimpled by a Gatan 656 dimple grinder to locate the electron beam–transparent area at the fusion zone, or the heat-affected zone of interest. Final electropolishing was performed in a Tenupol-3 twin-jet polisher using an electrolyte of 65 pct methanol, 30 pct butan-l-ol, and 5 pct perchloric acid, maintained at −35° C, and a d.c. voltage of 30 V. Microstructures were examined in a JEOL 2000FX TEM/scanning TEM operating at an accelerating voltage of 200 kV. Because the weld fusion zone exhibits a dendrite structure, it was not possible to evaluate the volume fraction of phase-transformation product that was produced during welding by optical microscopic imaging. Therefore, a minimum of six thin foils were prepared from each weld, and about 15 TEM bright-field images were taken at a magnification of 20,000 times from each thin foil to determine the volume fraction of retained α phase.

III. RESULTS

As shown by optical micrographs in Figures 1(a) and (b), both as-received Ti-45Al-2Nb-2Mn and Ti-48Al-2Nb-2Mn parent materials had a fully lamellar microstructure consisting of α_2 and γ laths.

Figure 2 shows a typical example of cracks seen in the top surface of the Ti-45Al-2Nb-2Mn alloy weld made at a calculated cooling rate of 1670 °C/s. It is seen that the cracks were transverse across the fusion zone and propagated extensively into the base material at approximately 45 deg from the welding direction (Figure 2). No evidence of grain-boundary liquation or other features associated with hot cracking were observed in this study. With a decrease in the weld cooling rate, the weld cracking became less severe, as

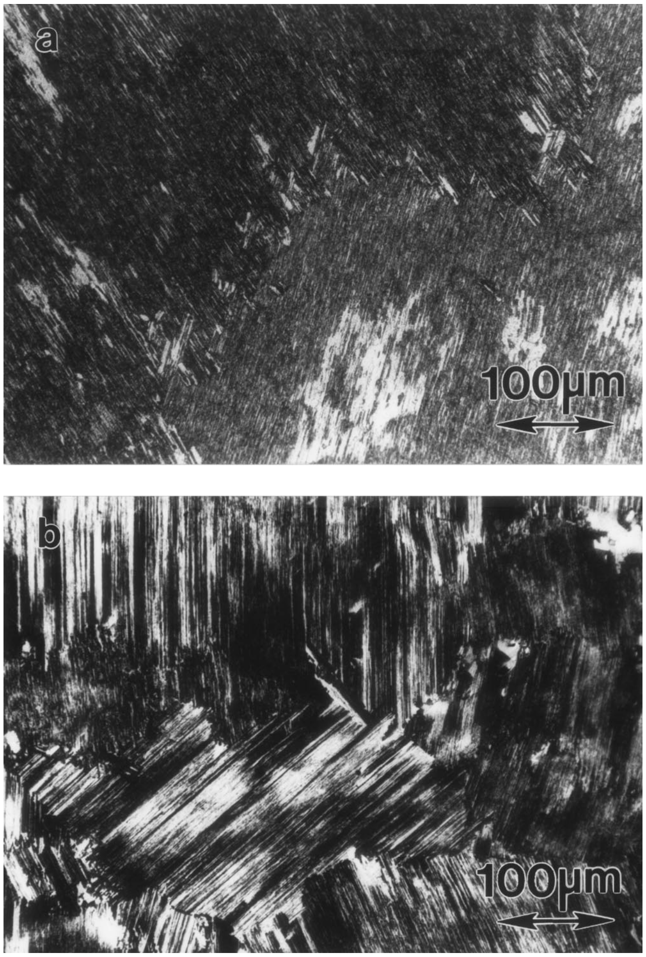

Fig. 1—Optical micrographs showing fully lamellar structure in the (*a*) Ti-45Al-2Nb-2Mn and (*b*) Ti-48Al-2Nb-2Mn parent materials.

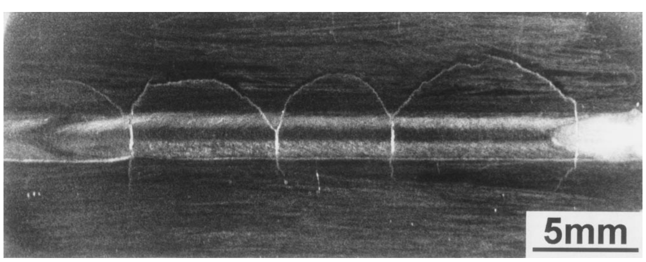

Fig. 2—Optical photographs of an electron beam weld of the Ti-45Al-2Nb-2Mn alloy made at a cooling rate of 1670 °C/s.

seen in Figure 3, which shows values of crack frequency as a function of the calculated weld cooling rate. It should be noted that a sharp decrease in crack frequency occurs at a cooling rate of around 660 °C/s, and the crack frequency increases almost linearly with weld cooling rates above 730 °C/s and below 590 °C/s. Since higher cooling rates would result in a higher temperature gradient in the weld and, accordingly, greater thermal stresses, the thermally induced residual stresses would cause the linear increase in cracking frequency with the cooling rate. However, if only the thermally induced stresses were responsible for the weld cracking, the sharp decrease in crack frequency should not have occurred when the cooling rate decreased to around 660 °C/s, as seen in Figure 3. It is, thus, reasonable to suggest that the material itself might have undergone fundamental change when the cooling rate was less than 660 °C/s, increasing the fracture strength or ductility of the material.

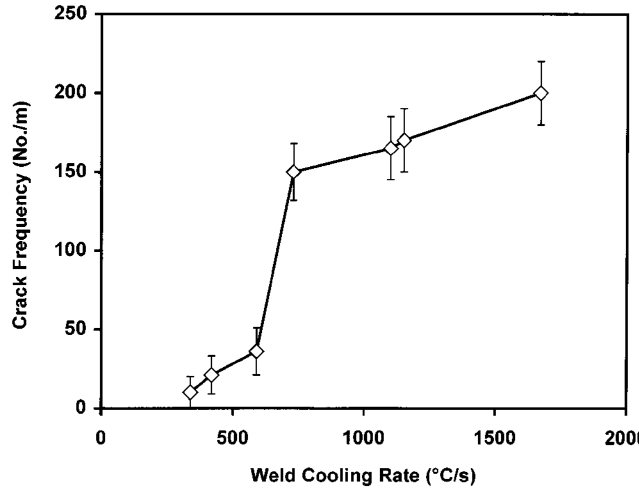

Fig. 3—Crack frequency *vs* calculated weld cooling rate.

The microstructures developed in the welds made at different cooling rates were characterized by the TEM. The EDS analysis did not show any change in composition in the welds, within the resolution limit of the technique. Therefore, composition variation would not have contributed to the microstructural change that occurred in the weld.

It was observed that the welds made at cooling rates of 730 °C or above contained a fully Al–supersaturated α_2 phase with a high density of stacking faults and antiphase domains (APDs). Figures 4(a) and (b) provide a bright-field image of the α_2 phase, with numerous stacking faults, and a central dark-field image of APDs in the α_2 phase, respectively, in the heat-affected zone of a weld made at a cooling rate of 1100 °C/s. It is seen that the high-temperature α phase in the weld did not decompose into γ phase; instead, it ordered into the α_2 phase during rapid cooling. It is known that Al-supersaturated α_2-Ti_3Al is extremely brittle and is undesirable. Therefore, the presence of an α_2 single phase might be the microstructural feature responsible for significant cracking of the welds made at a cooling rate of 730 °C/s or above. When the welds were made at a lower cooling rate, the high-temperature α phase in the heat-affected zone tended to transform into the γ phase through a massive transformation mechanism. Figure 5, which is a TEM microstructure of the heat-affected zone of a weld made at a cooling rate of 590 °C/s, shows the presence of a small fraction (approximately 7 pct) of massively transformed γ phase besides the α_2 phase, suggesting a partial suppression of the decomposition of α phase. The weld still showed the presence of solid-state cracking, but to a much smaller extent when the γ phase existed along with the retained α (α_2) phase than at higher cooling rates, where only the retained α (α_2) phase was present. It is, thus, suggested that weld cracking could be avoided when the decomposition of high-temperature α phase is not suppressed and the α phase fully transforms into the γ phase or α_2/γ lamellae. In order to obtain the desirable microstructure, it is necessary to cool slowly from the α-phase field by preheating the workpiece and/or slowing down the welding speed.

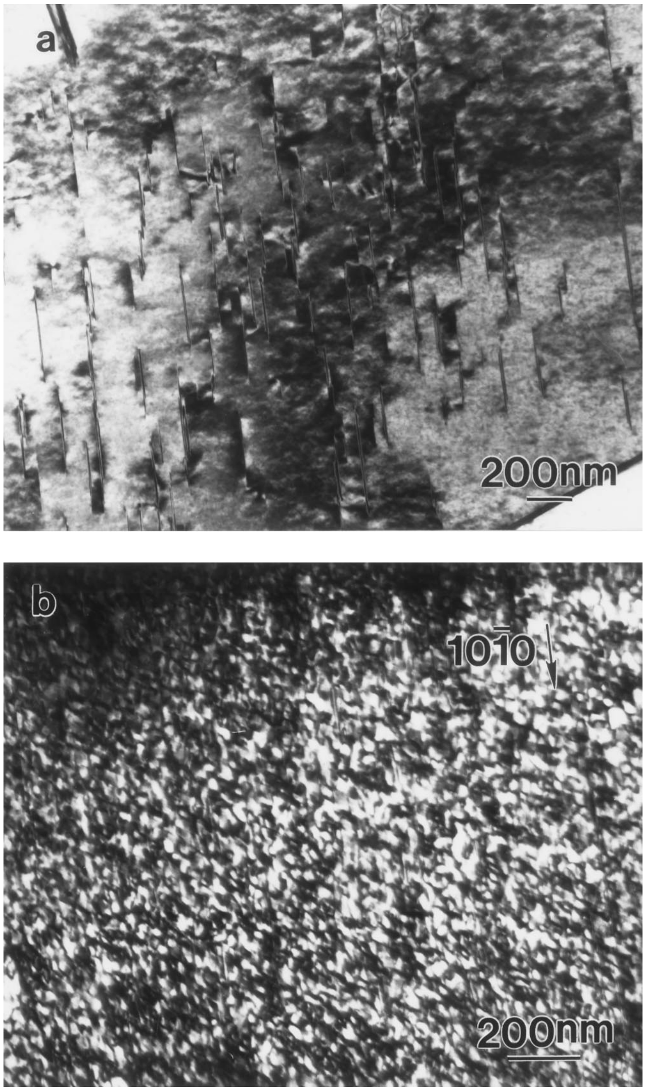

Fig. 4—TEM images showing that only α_2 phase was present at the heat-affected zone of a Ti-45Al-2Nb-2Mn weld made at a calculated cooling rate of 1100 °C/s. (*a*) Bright-field image where the stacking faults are edged-on. (*b*) Central dark-field image showing antiphase domains in the α_2 phase.

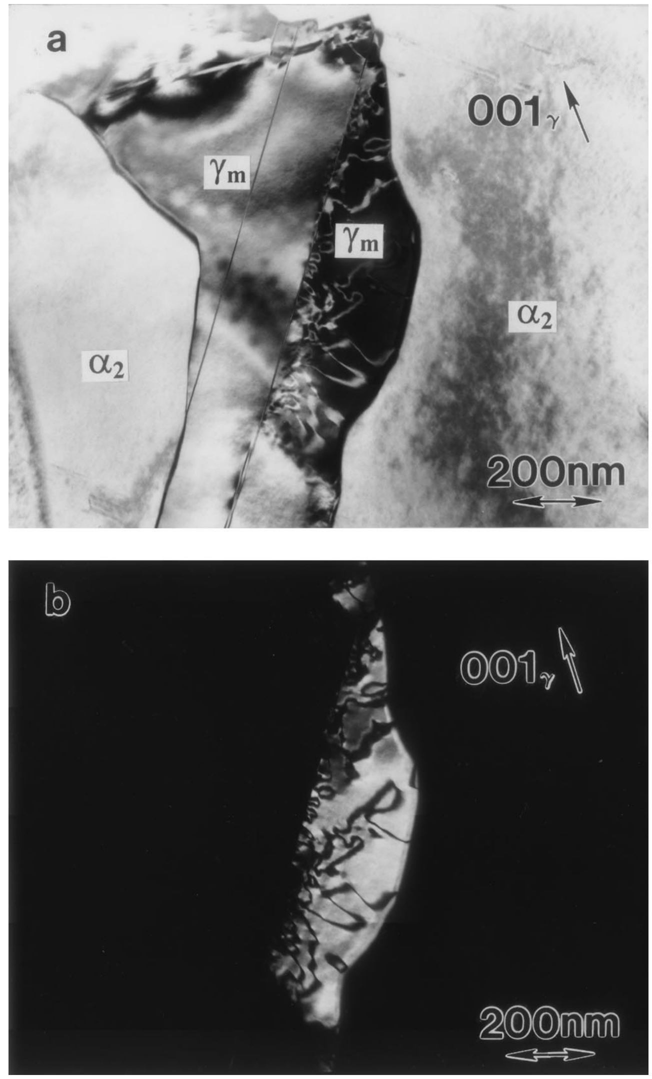

Fig. 5—TEM images showing the retained α (α_2) phase and massively transformed γ (γ_m) phase at the heat-affected zone of a Ti-45Al-2Nb-2Mn weld made at a calculated cooling rate of 590 °C/s. (*a*) Bright-field image and (*b*) central dark-field image showing antiphase boundaries in the γ_m phase. They were taken with **g** = (001) and the beam direction close to the [110] zone axis.

Figure 6 provides optical micrographs of microstructures of the Ti-45Al-2Nb-2Mn alloy specimens subjected to the GLEEBLE simulation. At very high cooling rates, the high-temperature α phase was entirely retained and only ordering of $\alpha \rightarrow \alpha_2$ took place, as shown in Figure 6(a). Cracks were observed in the sample, as indicated by arrows in Figure 6(a), which may be due to the brittleness of the retained α_2. With a decrease in the cooling rate, the massive transformation of $\alpha \rightarrow \gamma$ occurred (Figure 6(b)) while some of the α phase was still retained. It was found that the α phase decomposed fully into the α_2/γ lamellae and the massive γ phase at a cooling rate of 250 °C/s or less, as seen in Figure 6(c). At a slower cooling rate, the microstructure exhibited feathery and acicular features (Figure 6(d)).

Welding trials were then conducted with welding parameters which resulted in weld cooling rates of 240 °C/s and 270 °C/s. It was found that weld cracking did not occur at cooling rates of 240 °C/s, but was observed when the cooling rate was 270 °C/s. Optical photographs of the top surface and cross section of the crack-free bead-on-plate weld, made at the cooling rate of 240 °C/s, are shown in Figure 7. The TEM observations revealed that the heat-affected zone of this weld consisted of α_2/γ lamellae and massive γ phase, as seen in Figure 8.

In Figure 9, the weld-cracking frequency data are plotted as a function of weld cooling rate and volume fraction of the retained α phase in the weld. It is seen that the sharp drop in cracking frequency is almost directly related to the decrease in the volume fraction of retained α phase. The impact of volume fraction of retained α phase on the cracking frequency is also shown in Figure 10. It is seen that a sharp decrease in cracking frequency occurs as soon as α phase starts to transform and then gradually reduces to zero as the α phase is fully transformed. Therefore, it is concluded that the microstructure of the welds significantly influences the cracking frequency. However, welding stresses also play a role, albeit to a smaller extent.

Based on the welding parameters that were established

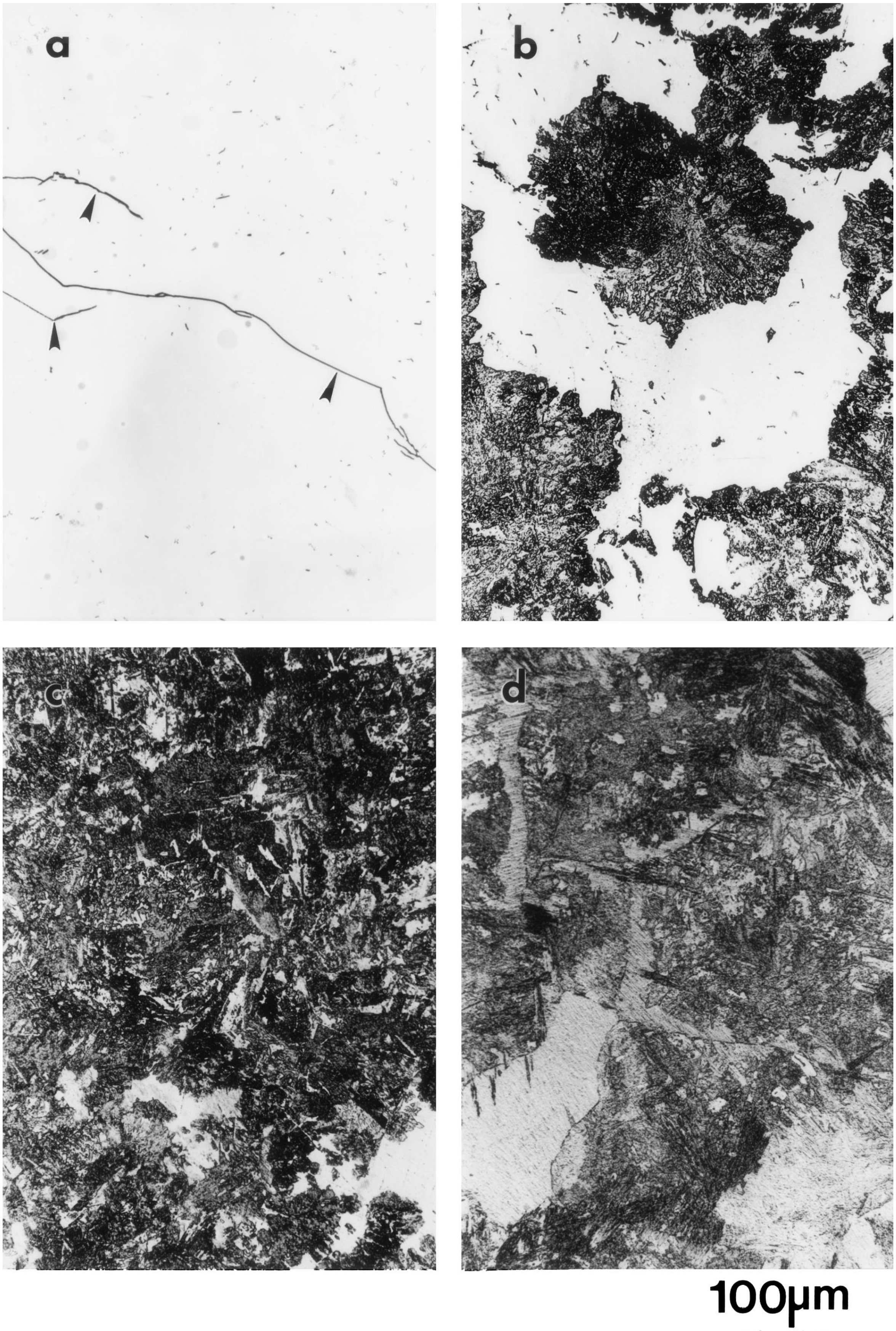

Fig. 6—Optical micrographs showing microstructures of the Ti-45Al-2Nb-2Mn alloy obtained by GLEEBLE simulation with different cooling rates: (*a*) 800 °C/s, (*b*) 500 °C/s, (*c*) 250 °C/s, and (*d*) 30 °C/s.

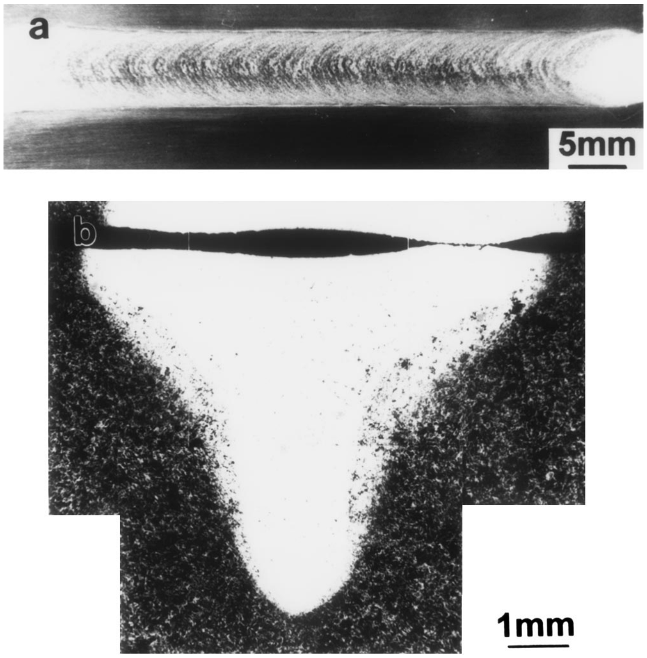

Fig. 7—Optical photographs of the (*a*) top surface and (*b*) cross section of a crack-free Ti-45Al-2Nb-2Mn weld made at a cooling rate of 240 °C/s.

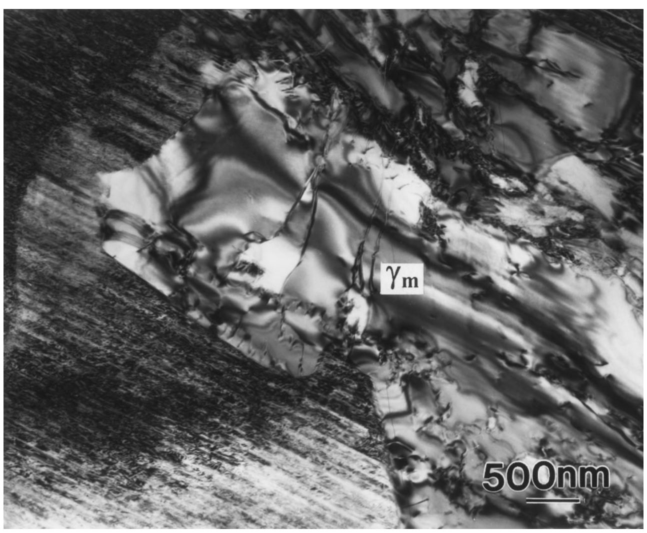

Fig. 8—TEM image showing the α_2/γ lamellae and the massive γ at the heat-affected zone of the Ti-45Al-2Nb-2Mn weld shown in Fig. 7.

using the bead-on-plate technique, butt welding was carried out on the Ti-45Al-2Nb-2Mn alloy with three sets of welding parameters, which gave rise to weld cooling rates of 200 °C/s, 240 °C/s, and 270 °C/s. It was found that crack-free welds were made only at a cooling rate of 240 °C/s or less. Figure 11 shows the top surface, bottom surface, and cross section of a crack-free butt weld made at a cooling rate of 240 °C/s.

To further confirm our hypothesis, a Ti-48A1-2Nb-2Mn alloy was also investigated. Before welding trials were carried out, GLEEBLE simulations were performed to determine the critical cooling rate at which the high-temperature α phase in the Ti-48A1-2Nb-2Mn alloy could fully decompose. At the highest cooling rate being used, the α phase

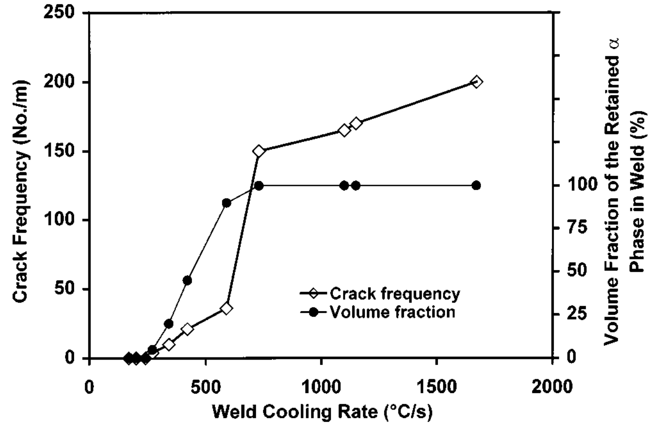

Fig. 9—Weld crack frequency and volume fraction of the retained α phase in the weld *vs* calculated cooling rate.

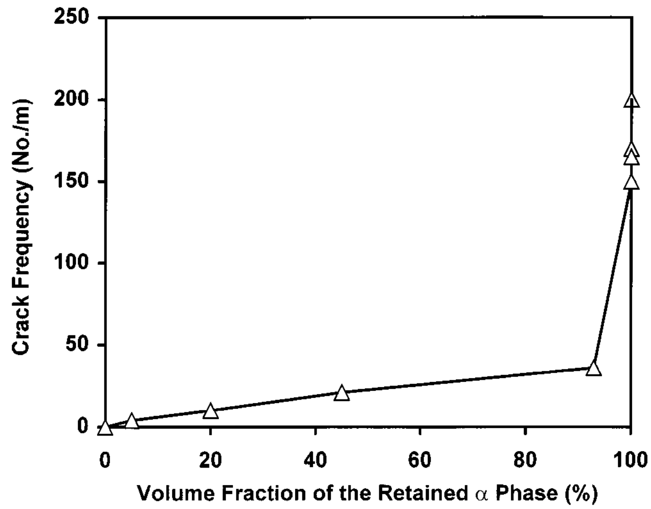

Fig. 10—Weld crack frequency as a function of volume fraction of the retained α phase in the weld.

was not entirely retained and, instead, it transformed partially into γ phase in a massive manner, as seen in Figure 12(a). When compared to Figure 6(a), it was found that the Ti-48A1-2Nb-2Mn alloy could undergo the $\alpha \rightarrow \gamma$ transformation more readily than the Ti-45Al-2Nb-2Mn alloy. It was observed that decomposition of the α phase was not suppressed until the cooling rate was reduced to about 400 °C/s (Figure 12(b)). With a further decrease in the cooling rate, the microstructure had a feathery and acicular morphology (Figure 12(c)) and, at very small cooling rates, well-defined α_2/γ lamellae formed (Figure 12(d)).

It is suggested that a crack-free weld in this alloy can be also obtained when the weld cooling rate was sufficiently low, less than 400 °C/s in this case, so that the α phase could fully decompose. Welding parameters were then selected to achieve weld cooling rates of 380 °C/s and 420 °C/s. It was observed that sound welds were made at cooling rates of 380 °C/s, but, for the welds made at the cooling rate of 420 °C/s, cracks were detected in the weld cross sections. Figures 13(a) through (c) show the top surface, bottom surface, and cross section, respectively, of a crack-free weld which was made at a cooling rate of 380 °C/s. The TEM observations confirmed that the microstructure of the weld was composed

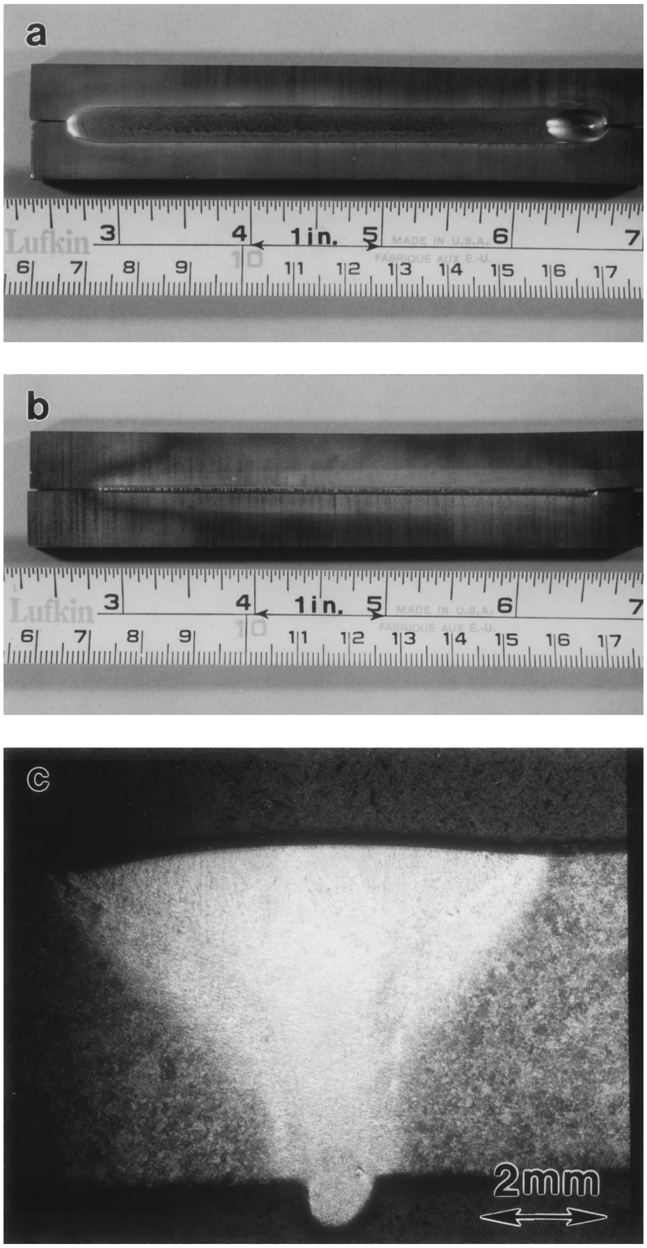

Fig. 11—Optical photographs showing the (*a*) top surface, (*b*) bottom surface, and (*c*) cross section of a crack-free butt weld made at a cooling rate of 240 °C/s.

of the α_2/γ lamellae and massive γ phase, as seen in Figure 14.

IV. DISCUSSION

The two alloys, Ti-45Al-2Nb-2Mn and Ti-48Al-2Nb-2Mn, should experience the same level of thermally induced stresses when welded under the same welding conditions, with higher cooling rates generating higher stresses. It has been established[14] that a lower Al content in the TiAl-based alloy increases the volume fraction of α_2 phase and, consequently, results in a higher strength. The tensile properties of the Ti-45Al-2Nb-2Mn and Ti-48Al-2Nb-2Mn alloys were not measured in this work. However, the tensile testing of similar alloys Ti-45Al-2Nb-2Mn + 0.8TiB$_2$ and Ti-47Al-2Nb-2Mn + 0.8TiB$_2$), both of which exhibit a fully lamellar structure, has indeed suggested that the lower-Al-content alloy has a higher yield strength than its higher-Al-content counterpart.[15] The Ti-45Al-2Nb-2Mn alloy is, thus, expected to be stronger than the Ti-48Al-2Nb-2Mn alloy and, consequently, should be able to sustain higher residual stresses. Therefore, it appears that the fact that a crack-free weld could be produced on the Ti-48Al-2Nb-2Mn alloy using a higher cooling rate (in other words, under higher residual stresses) than that in the Ti-45Al-2Nb-2Mn alloy cannot be explained on the basis of the strength of alloys and the residual stresses. Furthermore, as seen in the preceding section, residual stresses are not the primary factor that contributes to the weld cracking. Instead, microstructural changes that occur during welding more significantly affect the susceptibility of these two alloys to solid-state cracking. It has been qualitatively documented in the literature[16] and observed in this study that, depending upon the alloy composition, cooling rate, and grain size, in a Ti-(45–48)Al–based alloy, the nature and volume fraction of transformation products vary widely when it is cooled to room temperature from the high-temperature α-phase field. At slower cooling rates, the α phase transforms into a well-defined α_2/γ lamellar structure and a Widmanstatten, feathery, and/or acicular-type microstructure appears at a medium-slow cooling rate. The massive transformation of $\alpha \rightarrow \gamma$ takes place at a higher cooling rate. At a very high cooling rate, the decomposition of α phase is suppressed in favor of ordering of the α phase into the α_2 phase. The present study suggests that welding of TiAl-based alloys should be conducted at cooling rates that will not suppress the decomposition of α phase. It, thus, appears that establishment of CCT diagrams for the alloys will be very valuable in the selection of suitable welding parameters. However, at present, reliable CCT diagrams are not available for quaternary TiAl alloys. Figures 15(a) and (b) show, schematically, the CCT diagrams for the binary Ti-45Al alloy and Ti-48Al alloy, respectively.[16] It should be noted that the occurrence of massive transformation of the $\alpha \rightarrow \gamma$ phase is not reported in the Ti-45Al binary alloy; however, this transformation was observed in the Ti-45Al-2Nb-2Mn quaternary alloy in this study. Therefore, the schematic CCT diagram for the Ti-45Al alloy has been modified for the Ti-45Al-2Nb-2Mn alloy by adding an $\alpha \rightarrow \gamma$ massive transformation curve (the dashed curve in Figure 15(a)).

An examination of the CCT diagrams of TiAl alloys, shown in Figure 15, suggests that, in order to allow the α phase to transform completely into the α_2/γ lamellae and massive γ phase, the cooling curve has to pass through the right-hand side of the nose of the C-curve for $\alpha \rightarrow \alpha + \gamma$ transformation. Therefore, any factor that can move the C-curve of $\alpha \rightarrow \alpha + \gamma$ transformation to a shorter time will allow the material to be welded at higher cooling rates and, accordingly, will increase the weldability of the material. The higher aluminum content of the TiAl alloy tends to move the C-curve to a shorter time, thereby decreasing the risk of formation of Al-supersaturated retained α (α_2) phase and, thus, weld cracking. A higher-aluminum-content TiAl-based alloy will, therefore, be less problematic from a welding point of view, as it was observed in this study that crack-free welds could be produced on the Ti-48Al-2Nb-2Mn alloy at higher cooling rates than in the Ti-45Al-2Nb-2Mn alloy, *i.e.*, a lower preheating temperature was required for the Ti-48Al-2Nb-2Mn alloy.

The effects of alloying elements on the $\alpha \rightarrow \alpha + \gamma$

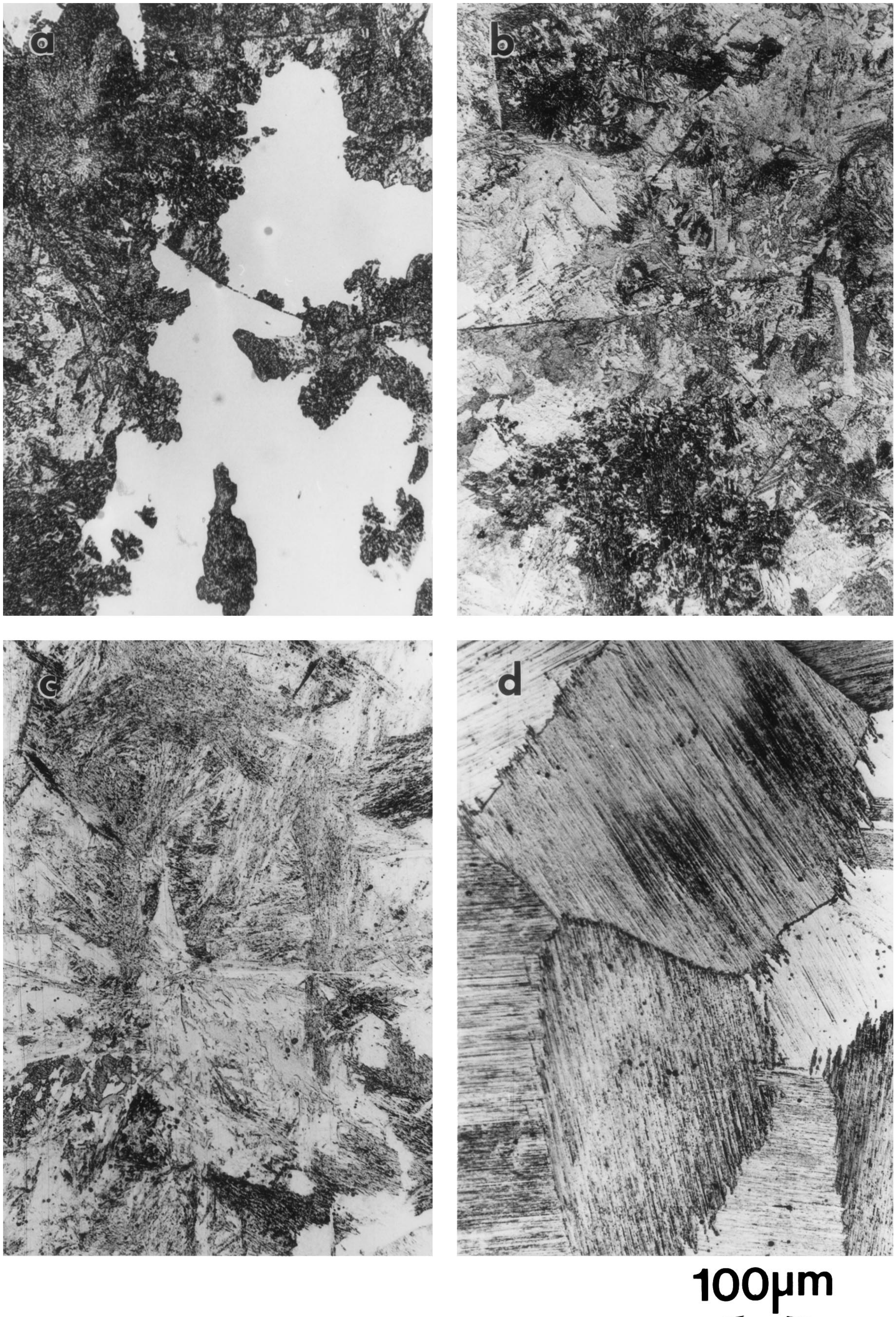

Fig. 12—Optical micrographs showing microstructures of the Ti-48Al-2Nb-2Mn alloy obtained by GLEEBLE simulation with different cooling rates: (*a*) 800 °C/s, (*b*) 400 °C/s, (*c*) 200 °C/s, and (*d*) 0.2 °C/s.

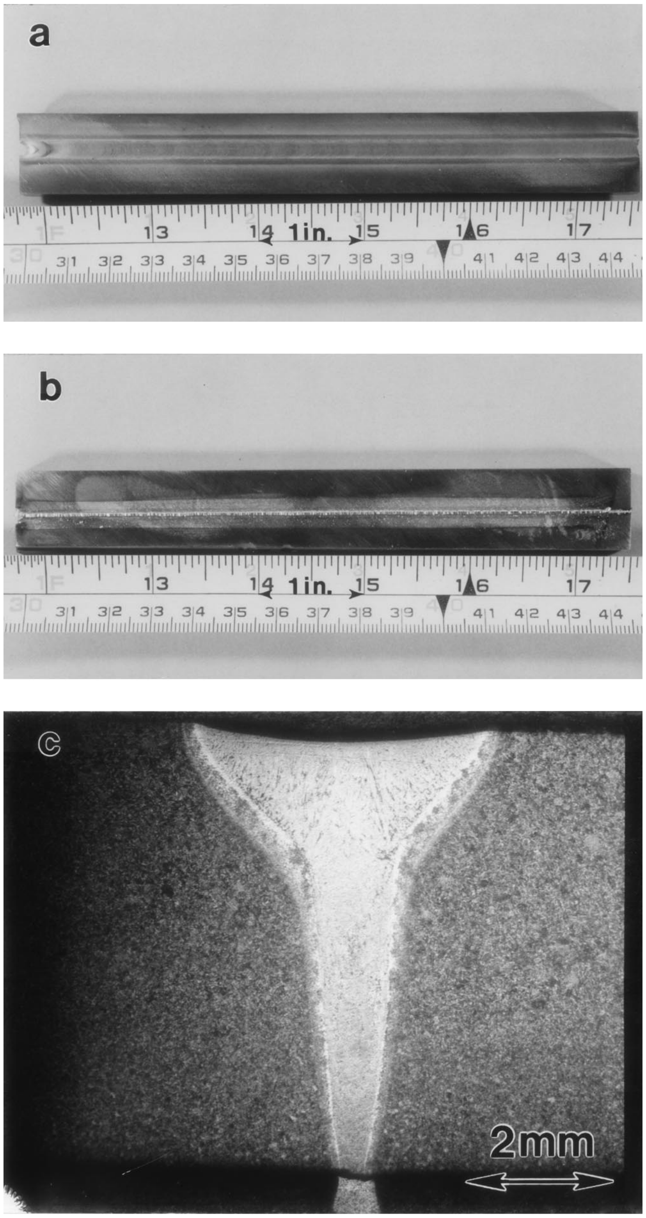

Fig. 13—Optical photographs showing the (*a*) top surface, (*b*) bottom surface, and (*c*) cross section of a crack-free weld, which was made at a cooling rate of 380 °C/s.

transformation have yet to be fully established. It should be noted that the weldability of a carbon or low-alloy steel is usually expressed in terms of a carbon-equivalent limit (C_{equiv}),[12] or maximum value. As a general rule, a steel is considered weldable if $C_{equiv} < 0.4$.[17] Similarly, an aluminum-equivalent limit (Al_{equiv}) could be developed for the welding practice of the TiAl-based alloys. Its value could be assessed in terms of how the alloying elements present affect the transformation characteristics, *i.e.*, whether the C-curve of the CCT diagram moves to longer or shorter times. In effect, the Al_{equiv} could provide an indication of the type of microstructure to be expected in the weld heat-affected zone, as a function of the cooling rate, and could be used as a guide for the selection of welding parameters.

The initial α grain size also influences the cooling rate–dependency of the microstructure. It was found[18] that small-grained materials had much faster transformation kinetics than the large-grained materials. With a decrease in the grain size, the C-curves of CCT diagrams may shift to a shorter time and, thus, the weldability of TiAl alloys may increase. In addition, oxygen is a very effective α stabilizer. An increase in oxygen concentration will displace the C-curve of the $\alpha \rightarrow \alpha + \gamma$ transformation to longer times, thus increasing the risk of weld cracking. However, systematic research is needed to quantify it.

Fig. 14—TEM image showing the α_2/γ lamellae and the massive γ at the heat-affected zone of the Ti-48Al-2Nb-2Mn weld shown in Fig. 13.

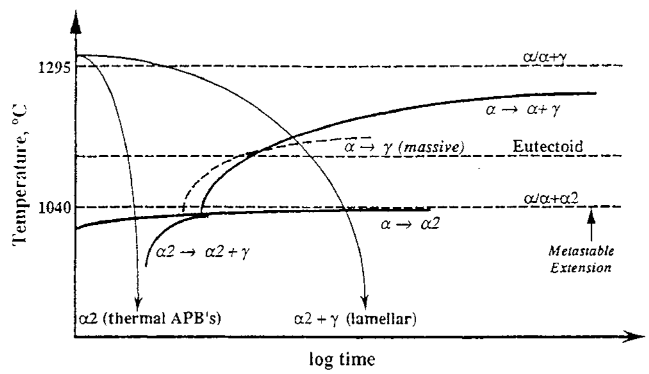

(*a*)

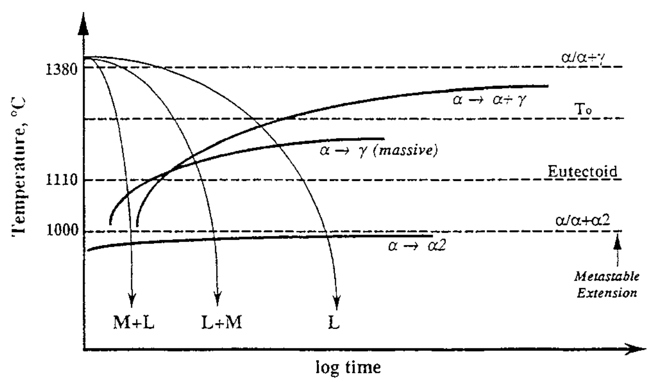

(*b*)

Fig. 15—Schematic CCT diagrams for a (*a*) Ti-45Al alloy and (*b*) Ti-48Al alloy representing the decomposition of the high-temperature α phase. M = massive, and L = lamellar.[16]

V. CONCLUSIONS

1. The Ti-45Al-2Nb-2Mn alloy and the Ti-48Al-2Nb-2Mn alloy were observed to be susceptible to solid-state cracking, which could, to a large extent, be attributed to the brittleness of the transformation products that formed during the electron-beam welding process.
2. A crack-free weld could be made if decomposition of the high-temperature α phase was not suppressed during welding.
3. The Ti-48Al-2Nb-2Mn alloy was found to be less susceptible to solid-state cracking than the Ti-45Al-2Nb-2Mn alloy.
4. A CCT diagram is suggested to be a valuable reference for selection of welding parameters to produce crack-free weld.

ACKNOWLEDGMENTS

The authors thank the consortium of Manitoba Aerospace Industries and NSERC of Canada for their financial support. They are grateful to John Davise, Bristol Aerospace Ltd., and John Van Dorp and Don Mardis, University of Manitoba, for their technical assistance. They also acknowledge Dr. H. Guo for his help with the GLEEBLE simulation.

REFERENCES

1. R.A. Patterson, P.L. Martin, B.K. Damkroger, and L. Christodoulou: *Weld. J.*, 1990, vol. 69 (1), pp. 39-s-44-s.
2. P.L. Threadgill: *Mater. Sci. Eng. A*, 1995, vols. A192–A193, pp. 640-46.
3. M.C. Chaturvedi, N.L. Richards, and Q. Xu: *Mater. Sci. Eng. A*, 1997, vols. A239–A240, pp. 605-12.
4. C.M. Austin, T.J. Kelly, K.G. McAllister, and J.C. Chesnutt: in *Structural Intermetallics*, M.V. Nathal, R. Darolia, C.T. Liu, P.L. Martin, D.B. Miracle, R. Wagner, and M. Yamaguchi, eds., TMS, Warrendale, PA, 1997, pp. 413-25.
5. V. Acoff and D. Bharani: *Proc. Materials Solution'97 on Joining and Repair of Gas Turbine Components*, [Indianapolis, IN,] ASM International, OH, 1997, pp. 137-42.
6. H. Clemons, N. Eberhardt, W. Glatz, H.P. Martinz, W. Knabl, and N. Reheis: in *Structural Intermetallics*, M.V. Nathal, R. Darolia, C.T. Liu, P.L. Martin, D.B. Miracle, R. Wagner, and M. Yamaguchi, eds., TMS, Warrendale, PA, 1997, pp. 277-86.
7. W.A. Baeslack III, P.L. Threagill, E. D. Nicholas, and T.F. Broderick: in *Titanium'95: Science and Technology,* P.A. Blenkinsop, W.J. Evans, and H.M. Flower, eds., The Institute of Materials, London, United Kingdom, 1996, pp. 424-31.
8. W.A. Baeslack III, H. Zhang, P.L. Threagill, and B.G.I. Dance: *Mater. Characterization*, 1997, vol. 39, pp. 43-52.
9. G. Çam, K.-H. Bohm, J. Mullauer, and M. Koçak: *JOM*, 1996, No. 11, pp. 66-68.
10. P. Yan and E.R. Wallach: *Intermetallics*, 1993, vol. 1, pp. 83-97.
11. Q. Xu, M.C. Chaturvedi, N.L. Richards, and N. Goel: in *Structural Intermetallics*, M.V. Nathal, R. Darolia, C.T. Liu, P.L. Martin, D.B. Miracle, R. Wagner, and M. Yamaguchi, eds., TMS, Warrendale, PA, 1997, pp. 323-29.
12. K. Easterling: in *Introduction to the Physical Metallurgy of Welding*, 2nd ed., Butterworth-Heinemann, London, 1992.
13. M. Yamaguchi and H. Inui: in *Structural Intermetallics*, R. Darolia, J.J. Lewandowski, C.T. Liu, P.L. Martin, D.B. Miracle, and M.V. Nathal, eds., TMS, Warrendale, PA, 1993, pp. 127-42.
14. S.-C. Huang and D.S. Shih: in *Microstructure/Property Relationships in Titanium Aluminides and Alloys*, Y.W. Kim and R.R. Boyer, eds., TMS, Warrendale, PA, 1990, pp. 105-22.
15. Y.W. Kim and D.M. Dimiduk: in *Structural Intermetallics*, M.V. Nathal, R. Darolia, C.T. Liu, P.L. Martin, D.B. Miracle, R. Wagner, and M. Yamaguchi, eds., TMS, Warrendale, PA, 1997, pp. 531-43.
16. S.A. Jones and M.J. Kaufman: *Acta Metall. Mater.*, 1993, vol. 41(2), pp. 387-98.
17. "Guide to the Welding and Weldability of C-Mn Steels and C-Mn Microalloyed Steels," International Institute of Welding, Paris, France, Publications Document II S/IIW-382-71, 1971.
18. L.L. Rothenflue and H.A. Lipsitt: in *Titanium'95: Science and Technology,* P.A. Blenkinsop, W.J. Evans, and H.M. Flower, eds., The Institute of Materials, London, United Kingdom, 1996, pp. 176-83